Influence of semiconductor/insulator/semiconductor structure on the photo-catalytic activity of Fe_3O_4/SiO_2/polythiophene core/shell submicron composite

Fan Zhang [a,*], Yuanji Shi [b], Zongshan Zhao [c], Weijie Song [d], Yang Cheng [e]

[a] College of Science, Nanjing Agricultural University, Nanjing 210095, PR China
[b] Nanjing Panda Electronics Co., Ltd., Nanjing 210000, PR China
[c] Key Laboratory of Marine Chemistry Theory and Technology, Ministry of Education, Ocean University of China, Qingdao 266100, PR China
[d] Ningbo Institute of Material Technology and Engineering, Chinese Academy of Sciences, Ningbo 315201, PR China
[e] College of Chemical Engineering and Technology, Wuhan University of Science and Technology, Wuhan 430083, PR China

ARTICLE INFO

ABSTRACT

The Fe_3O_4/SiO_2/polythiophene (FSP) submicron composite (SC) with a structure of semiconductor/insulator/semiconductor (SIS) was obtained. The characterization results showed that the FSP SC had a spherical core/shell shape with an average diameter of 506 nm. The high saturated magnetization value (~39 emu/g) ensured the easy separation of FSP SC from aqueous solution. The photo-catalytic activity of the FSP SC was evaluated by the degradation of methyl orange (MO) under UV-irradiation in the presence of H_2O_2. Due to the SIS structure, the degradation rate constant by FSP SC ($0.02177\,min^{-1}$) was 6.4, 1.6, and 2.5 times higher than that of Fe_3O_4/polythiophene (FP), polythiophene (P), and TiO_2, respectively. The repetition results suggested the good photochemical stability of FSP SC. The mechanism was proposed by investigating the energy band variation of the SIS structure, the transfer of light generated carriers and the formation of effective hydroxyl radicals in the photo-catalysis progress.

1. Introduction

Recently, polythiophene and its derivatives have been studied widely because of their moderate band gap, excellent electrical activity, low redox potential, photochemical, and thermal stability under photo-irradiation [1–4]. On the other hand, magnetite (Fe_3O_4) nanoparticle has also attracted much attention due to its super paramagnetic property ensuring the easy recovery in the presence of external magnetic field [5–7]. Therefore, the heterogeneous materials, which have the properties of both polythiophene (or its derivatives) and Fe_3O_4 particles, can be exploited for photocatalysis applications. However, few studies of this composite as photo-catalyst have been reported to our best knowledge. Jang et al. synthesized the core/shell nanocomposite of Fe_3O_4/poly(3,4-ethylenedioxythiophene) in the presence of strong acid (HCl), which showed attractive prospects for the photo-catalytic degradation of organic dyes [8]. Nevertheless, there are still some problems: (i) the instability of Fe_3O_4 in the as-prepared composite as a result of usage of strong acid; (ii) the demand of a high magnetic field in the reclaiming process due to the low saturated magnetization of the composite. So the stability and the magnetization value are still deserved to promote to meet the actual demand in application.

Furthermore, p–n hetero-junction is known to be beneficial to the separation of the photo-electrons and holes, which can enhance the photo-catalytic efficiency [9]. However, few studies have introduced the performance of polythiophene (energy gap 2.0 eV) and Fe_3O_4 (energy gap 0.14 eV) as the p and n type semiconductor, respectively [10–12]. In addition, the semiconductor/insulator/semiconductor (SIS) structure is also helpful for the separation of the photo-electrons and holes which has been widely used in the field of solar cells [13–15]. The employment of SiO_2 as the insulating shell to participate in the catalyst formation with a SIS structure has been seldom reported though it was usually introduced as the protected or connected shell [16–18]. It enlightens us to develop the materials with a SIS structure as novel photo-catalysts.

In this study, the n-Fe_3O_4/SiO_2/p-polythiophene (FSP) submicron composite (SC) with a core/shell and SIS structure was synthesized. The photo-catalytic properties of the obtained FSP SC was evaluated for the decoloration of methyl orange (MO) with H_2O_2 under UV-irradiation. It is anticipated that the
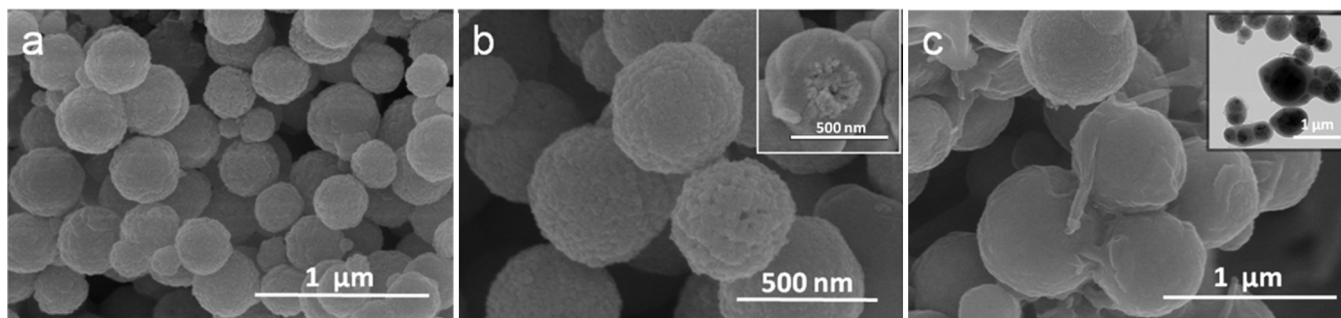
Fig. 1. SEM images of (a) Fe_3O_4, (b) FS (inset: magnified image of a cracked FS core/shell SC), (c) FSP SC (inset: TEM image of FSP core/shell SCs).

well-defined structure of FSP SC can provide the advantages such as the enhancement of photo-catalytic performance, the environmental protection of iron oxide, the easy magnetic recovery, and the repeated usage.

2. Experiments

2.1. Chemicals and instrumentation

Thiophene monomer, tetrachloromethane (CCl_4), anhydrous ferric chloride ($FeCl_3$), iron(III) chloride hexahydrate ($FeCl_3·6H_2O$), sodium acetate (NaAc), polyethylene glycol 2000 (PEG2000), ethylene glycol, tetraethoxysilane (TEOS), ammonium hydroxide ($NH_3·H_2O$), oxydol (H_2O_2, 30%), methyl orange (MO), and isopropyl alcohol were all purchased from the Shanghai Sinopharm Chemical Reagent Co., Ltd (China). All the reagents were of analytical grade and used as received without further treatment. P25 (nanoscale TiO_2 powder, surface area 50 m^2/g) was purchased from the Degussa AG of Germany. The MO solution (1000 ppm) was prepared by adding 0.1 g MO powder into 100 mL distilled water.

The as-prepared composite powder was characterized in detail as follows. The morphology of the as-prepared materials was observed using a scanning electron microscopy (SEM, Model S-4800, Hitachi Limited, Japan) and a transmission electron microscope (TEM, Model Tecnai F20, FEI, USA). The functional groups of the composites were examined through a Fourier transform infrared spectroscopy (FTIR, Nicolet 6700, Thermo, USA) using a KBr pressed disk. The elements and composition were studied by an X-ray photoelectron spectroscope (XPS, Axis Utltradld, Shimadzu, Japan). The crystal structure was determined by an X-ray diffraction (XRD) analyses on a Bruker (Germany) AXS Model D8 Advance X-ray diffractometer (Cu $K\alpha$ radiation, $\lambda = 0.15406$ nm). The magnetic performance of FSP was investigated by a physical property measurement system (PPMS, Model-9, Quantum Design, USA). The degassing was performed at 180 °C for 300 min prior to performing the N_2 adsorption experiment. The surface area was calculated by Brunauer–Emmett–Teller (BET) equation. The average particle size was estimated by the Zeta potential analyzer (Nano ZS, Malvern, England). The degree of MO degradation was determined by an all cross-references microplate reader (F1-01621, Thermo, Finland). The effective radical that presented in the degradation process was detected by an electron spin resonance (ESR, ESR300E, Bruker, Germany).

2.2. Preparation of the products

The Fe_3O_4 core with a diameter of ~400 nm was prepared using a solvothermal method. Then, the Fe_3O_4/SiO_2 (FS) composite was obtained by TEOS hydrolysis in alkalic condition on the surface of Fe_3O_4 submicron particles. The detail of synthesis process has been reported in our earlier work [16]. Furthermore, the as-prepared FS

composite was dispersed into 100 mL of CCl_4 and stirred for 30 min. Then, 0.4 mL of thiophene monomer was added into the mixture and the chemical oxidation polymerization was started by the addition of 3.1 g $FeCl_3$ as the oxidant at room temperature. After 4 h, the reaction was finished and the obtained black precipitation was collected by a permanent magnet. The as-obtained product was washed by deionized water and ethanol for three times, dried in a vacuum oven at 60 °C for 6 h. For comparison, Fe_3O_4/polythiophene (FP) and polythiophene (P) were also synthesized using the same method.

2.3. Photo-catalytic process

The photo-degradation of MO was carried out as follows. In a typical reaction system, it contained 50 mg/L MO, 40 mg/L catalyst, and 100 μL H_2O_2 to form a 50 mL mixed solution in a quartz glass. In the first 20 min, the mixture was stirred in the dark to reach the adsorption–desorption equilibrium and the concentration of MO left in the aqueous solution was defined as the initial concentration C_0. Then, the system was irradiated using a 16 W UV lamp at 365 nm. At intervals, 1.0 mL aqueous solution was sampled, filtered through a 0.45 μm pore size filter and determined at wavelength of 471 nm on an UV detector. The concentration was defined as C_t and the ratio of C_t/C_0 was taken as degradation efficiency.
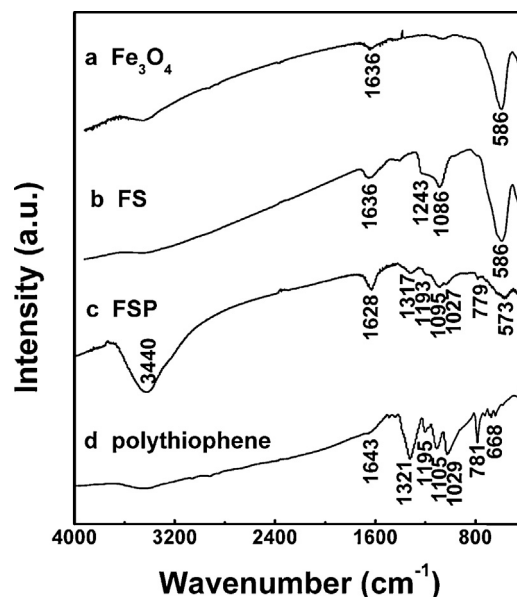
Fig. 2. FTIR spectrum of (a) Fe_3O_4, (b) FS, (c) FSP SC, and (d) polythiophene.

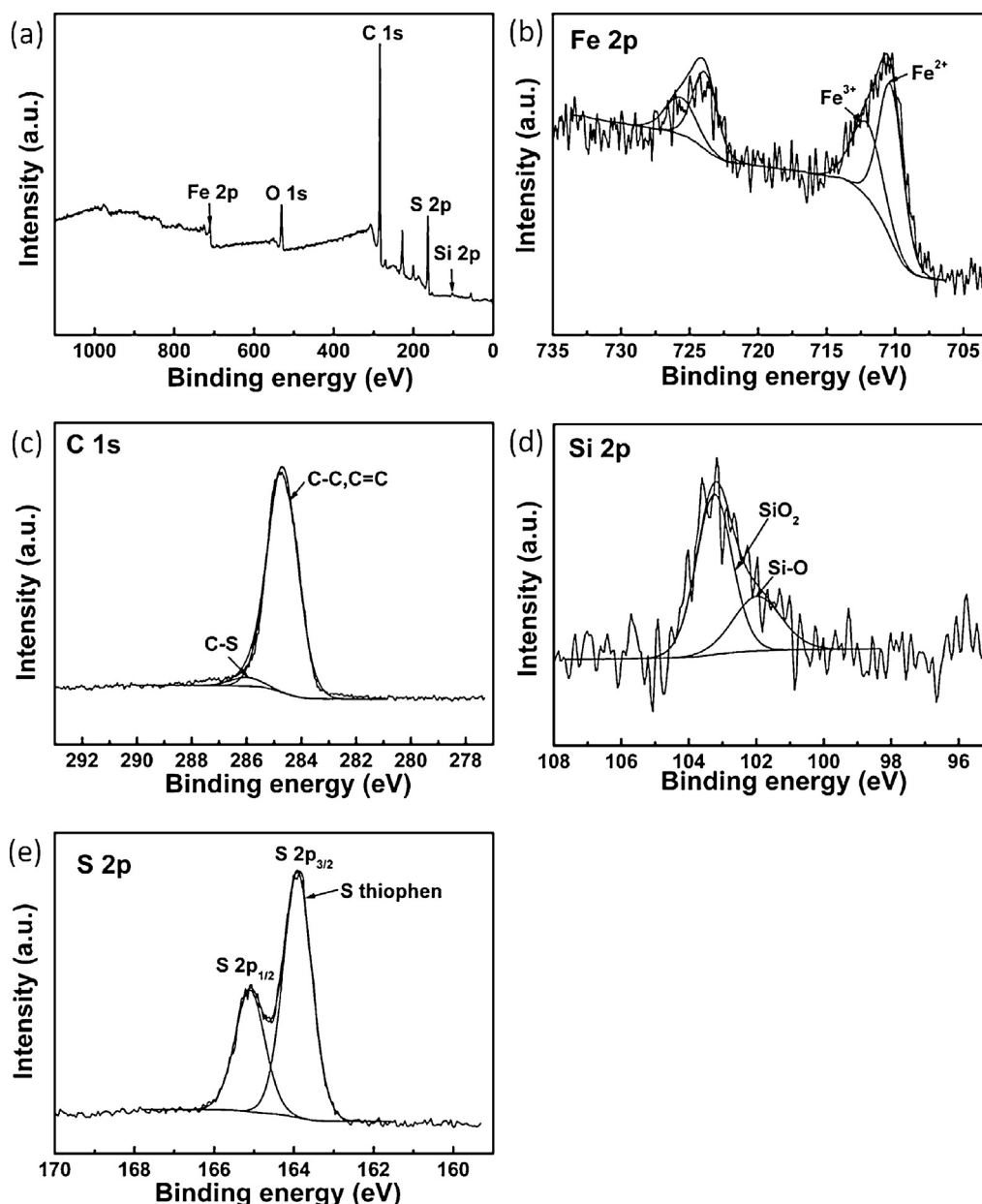Fig. 3. XPS spectra of FSP: (a) survey spectra; (b) Fe 2p; (c) C 1s; (d) Si 2p; (e) S 2p.

3. Results and discussion

3.1. Characterization

The SEM images of Fe_3O_4, FS, and FSP are shown in Fig. 1. Their diameters increased with the further formation of outside coatings while the shape maintained. The SiO_2 shell was closely encapsulated on the surface of Fe_3O_4 (the inset to Fig. 1b). As seen in Fig. 1c, FSP SC was successfully prepared with an average diameter of 500 nm and the TEM image (the inset to Fig. 1c) showed the core/shell structure of FSP SC.

The FTIR analysis was used to investigate the composition of the as-prepared Fe_3O_4, FS, FSP, and polythiophene (Fig. 2). The Fe–O stretching vibration peak of Fe_3O_4 at 573 cm^{-1} [5] confirmed the existence of Fe_3O_4 in the FSP SC. The adsorption bands at 1243 cm^{-1} and 1086 cm^{-1} were assigned to the characteristic vibration of SiO_2 [16]. The peak at 3440 cm^{-1} was the stretching vibration of the OH group [17]. The C=C characteristic stretching vibration peak

of polythiophene at 1643 cm^{-1} [12] indicated the formation of polythiophene in FSP SC. The C–H out-of-plane stretching vibration peak at 781 cm^{-1} of the 2,5-substituted thiophene ring was also present [19]. When polythiophene was coated on FS SC, the characteristic absorption peaks of polythiophene at 1643 cm^{-1}, 1321 cm^{-1}, 1195 cm^{-1}, 1105 cm^{-1}, and 1029 cm^{-1} were blue-shifted to 1628 cm^{-1}, 1317 cm^{-1}, 1193 cm^{-1}, 1095 cm^{-1}, and 1027 cm^{-1}, respectively. This could be attributed to the decrease of electron density in polythiophene chain [20] which resulted from the interaction between polythiophene and FS SC [12].

The chemical information on the surface of FSP SC was investigated via XPS analysis (Fig. 3). The main peaks on behalf of Fe_3O_4, polythiophene and SiO_2 all appeared in the XPS spectra of FSP (Fig. 3a). The main peaks of Fe $2p_{3/2}$ (Fig. 3b) core-line spectra at 710.5 eV and 712.2 eV were assigned to be Fe^{2+} and Fe^{3+}, respectively, indicating the existence of Fe_3O_4 [21]. The main peaks of C 1s core–line spectra (Fig. 3c) at 284.8 eV and 286.1 eV were associated with C–C/C=C and C–S in the presence of

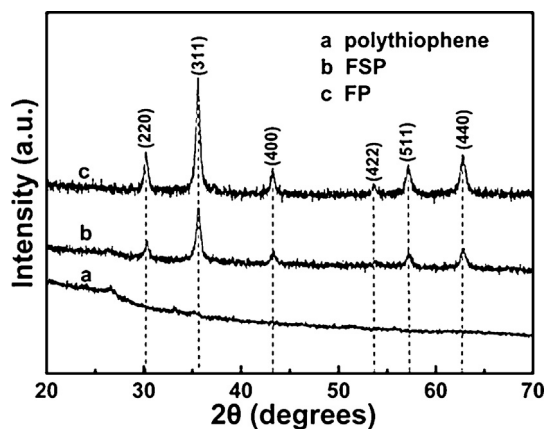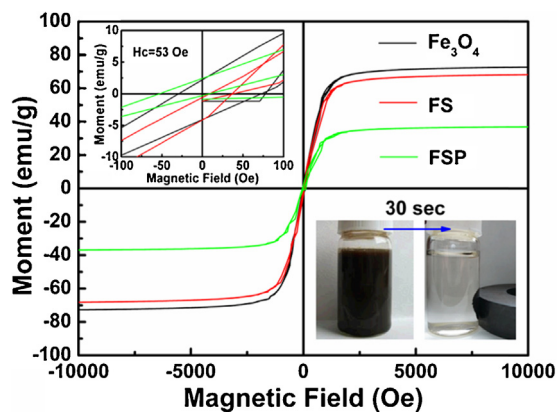**Fig. 4.** XRD patterns of (a) polythiophene, (b) FSP, (c) FP SC.

Fig. 5. The magnetic performance of Fe_3O_4, FS and FSP SCs with the expanded hysteresis loop (inset). The inner photographs indicate that FSP SC in the aqueous solution can be attracted and arranged vertically by a magnetic coil.

polythiophene, respectively [22]. The peaks at 101.9 eV and 103.2 eV in Fig. 3d were due to Si–O and SiO_2, respectively, representing SiO_2 [21]. The S 2p spectra (Fig. 3e) was composed of $2p_{3/2}$ and $2p_{1/2}$ peaks with an intensity ratio of 2:1, as theoretically determined from the spin–orbit splitting effect [23,24]. The thiophene sulfur peak presented at around 164 eV [24]. These results suggested that the obtained material was composed of Fe_3O_4, SiO_2 and polythiophene, as we described in the synthesis process.

The X-ray diffraction (XRD) patterns of the pure polythiophene, Fe_3O_4/polythiophene (FP), and the FSP SC are shown in Fig. 4. Only a broad peak at the 2θ value of 20–30° appeared for pure polythiophene (Fig. 4a), indicating its amorphous phase. In the case of FP (Fig. 4c), six peaks at about 30.3°, 35.6°, 43.2°, 53.4°, 57.2°, and 62.7° were due to the diffraction of (2 2 0), (3 1 1), (4 0 0), (4 2 2), (5 1 1), and (4 4 0) planes of the face-centered cubic phase of Fe_3O_4, respectively, suggesting the formation of Fe_3O_4 crystal in the FP SC [25]. The intensity of Fe_3O_4 peak in FSP SC (Fig. 4b) decreased obviously compared with that in the FP SC, which was due to the addition of SiO_2 shell. The absence of SiO_2 peaks revealed the amorphous phase of SiO_2 in FSP SC [26]. These XRD results suggested that no other impurity in crystal phase was existed in the FSP SC. In addition, the Fe_3O_4 crystal was successfully used as the core where the intensity of its characteristic peaks decreased with the thickness of coated shell increased.

The recycling of photo-catalysts used in the remediation of polluted water is an important issue, because they will become new pollutant sources when left in the treating system. The as-prepared materials in this study could be magnetically reclaimed and their magnetic properties are shown in Fig. 5. For Fe_3O_4, FS, and FSP SC, there presented a hysteresis and the coercive force of 53 Oe indicated their super paramagnetic behavior, ensuring the recycling convenience. Their magnetization values increased quickly when the external magnetic field improved from 0 Oe to 2000 Oe and then reached saturated. Compared the saturation magnetization (Ms) values of the Fe_3O_4 (72 emu/g), FS (69 emu/g), and FSP SC (39 emu/g), there existed a decrease with the decreased content of Fe_3O_4 crystal. However, the Ms values of as-prepared products were still higher than those of other similar reports [8,17]. Therefore, these materials were easily separated from the aqueous solution within 30 s with only 1.3 wt% left (the inset to Fig. 5).

3.2. Photo-catalytic activities on MO

The photo-catalytic degradation of MO solution by the as-prepared materials is shown in Fig. 6a. The results showed that, only 10%, 25% and 46% of MO molecules were decomposed within 120 min in the presence of bare FSP, H_2O_2 or TiO_2 (curve a, b and e).

But with the addition of both FSP and H_2O_2 into the MO aqueous solution, the degradation rate was enhanced markedly with ~92% removed in 120 min (curve h), higher than that of the photo-catalyst TiO_2 with H_2O_2 (~65%, curve f). This confirmed that the $^\bullet$OH generated from H_2O_2 would be well controlled by FSP, and the slow-release of $^\bullet$OH improved the use efficiency of $^\bullet$OH and avoided the annihilation phenomenon [27]. It has been reported that conjugated polymer could be used as photo-catalyst for the removal of pollutants [28]. Hence, the polythiophene (P) with H_2O_2 also showed a good photo-catalytic performance (curve g). However,
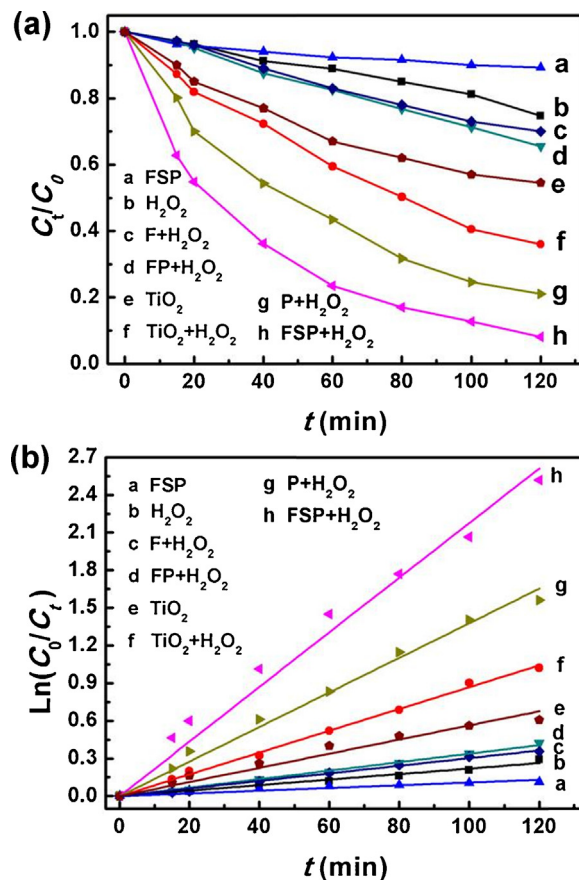

Fig. 6. The photo-catalytic kinetics of (a) bare FSP, (b) bare H_2O_2, (c) Fe_3O_4 with H_2O_2, (d) FP with H_2O_2, (e) bare TiO_2, (f) TiO_2 with H_2O_2, (g) P with H_2O_2, and (h) FSP with H_2O_2, under UV irradiation, $C_{(catalyst)}$ = 40 mg/L, $C_{(MO)}$ = 50 mg/L.

Table 1
The BET surface area and average particle size of different materials.

Material	BET surface area (m²/g)	Average particle size (nm)
F	23.7	382
FP	19.4	431
FSP	17.5	506
P	31.6	–
TiO_2 (P25)	50.2	21

Table 2
The rate constants of MO photo-degradation and linear regression coefficients from a plot of $\ln(C_0/C_t)$ versus t.

Photo-catalyst	k_{app} (min^{-1})	R^2
Bare FSP	0.00109	0.955
Bare H_2O_2	0.00220	0.991
F with H_2O_2	0.00304	0.997
FP with H_2O_2	0.00339	0.997
TiO_2	0.00564	0.987
TiO_2 with H_2O_2	0.00869	0.999
P with H_2O_2	0.01378	0.996
FSP with H_2O_2	0.02177	0.993

the removal efficiencies of MO by P, Fe_3O_4 (curve c) and FP (curve d) were all lower than that by FSP though these materials had the smaller size and bigger surface area (Table 1) which may be beneficial to improve the photo-catalytic performance. The better photo-catalytic performance of FSP should be due to its special SIS structure which was helpful for the separation of photo-generated electrons and holes, leading to the improved photo-catalytic activity.

The kinetics of photo-catalytic degradation of MO was well described by the apparent pseudo-first-order equation $\ln(C_0/C_t) = k_{app}t$, where k_{app} is the apparent rate constant, C_0 is the concentration of MO after darkness adsorption for 20 min and C_t is the concentration of MO at irradiation time t. Fig. 6b shows the linear relation of $\ln(C_0/C_t)$ versus irradiation time (t) for degradation of MO under different conditions. The determined rate constants (k_{app}) and linear regression coefficient (R^2) from these curves are presented in Table 2. All the kinetic data agreed well with the pseudo-first-order model because the R^2 values were higher than 0.95. The k_{app} values followed the sequence: FSP with H_2O_2 > P with H_2O_2 > TiO_2 with H_2O_2 > TiO_2 > FP with H_2O_2 > F with H_2O_2 > H_2O_2 > FSP. The introduction of SIS structure into the FSP composite could obviously enhance the H_2O_2-assisted photo-catalytic kinetics with a value of k_{app} (0.02177 min^{-1}). This value was 6.4, 1.6, and 2.5 times higher than that of FP, P, and TiO_2, respectively. In addition, the H_2O_2 and FSP played the role as co-catalysts in the degradation process which exhibited lower overpotential and higher catalytic activity [27,29].

3.3. Repetition

The photo-catalytic degradation of MO by FSP SC was carried out for ten cycles to evaluate its reusability. There was only 14% of decline in the tenth cycle relative to the first usage (Fig. 7). Furthermore, the *Ms* values also kept well and the separation was still realized within 30 s. The maintenance of these properties could be explained by the excellent photochemical stability of polythiophene [30], the protection of Fe_3O_4 core from oxidation and corrosion by coating shells [3,31]. And this has also been identified by the unchanged FTIR and XPS results of FSP before and after photo-degradation (not shown).

3.4. Photo-catalytic mechanism

In general, a semiconductor photo-catalytic cycle comprises three steps: first, illumination induces a transition of electrons
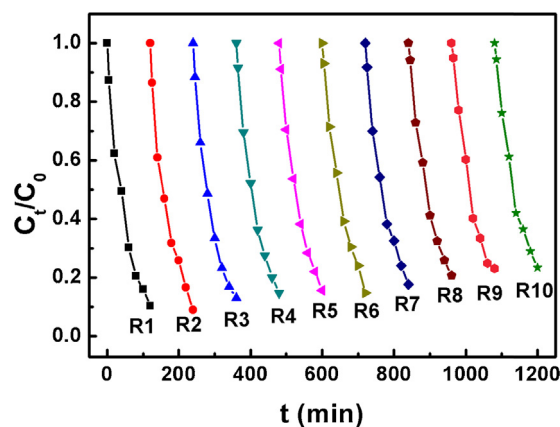
Fig. 7. Recycling experiments for the photo-degradation of MO by FSP SC.

from the valence-band (VB) to the conduction-band (CB), leaving an equal number of holes; second, the excited electrons (e$^-$) and holes (h$^+$) migrate to the surface of catalyst; third, they react with absorbed electron acceptors and electron donors, resulting in the photo-catalytic reaction [29].

The formation and the transfer of light generated electrons and holes are shown in Fig. 8. In the initial period of photo-catalytic reaction (Fig. 8a), the e$^-$ and h$^+$ can be generated in both Fe_3O_4 and polythiophene under the UV irradiation due to their n and p type semiconductor property, respectively. The electrostatic interaction between the generated e$^-$ in Fe_3O_4 and h$^+$ in polythiophene is helpful for their transference to the two interfaces of SiO_2 shell (marked 1 and 2 in Fig. 8a, respectively). Owing to the much larger thickness of SiO_2 shell than the desired one in the tunneling effect (about 0.1 nm) [32], the tunneling current is unable to achieve. However, the generated e$^-$ and h$^+$ in polythiophene can still be effectively separated, and the e$^-$ can transfer to the surface of polythiophene. Then, the adsorbed electron acceptors (mainly H_2O_2 here) can react with the e$^-$ on the surface of polythiophene shell, forming the active radicals ($^\bullet$OH and $^\bullet$O$_2^-$) which are responsible for the degradation of MO. In the later period of photo-catalytic reaction (Fig. 8b), the consumption of e$^-$ and the accumulation of h$^+$ in the *p*-polythiophene/SiO_2 interface will lower down the energy levels of *p*-polythiophene [33]. As the VB of *p*-polythiophene is lowered down to some level, at this time the photo-generated h$^+$ tends to transfer into the *p*-polythiophene/SiO_2 interface [33]. But the tunneling current is also impossible due to the barrier of thick SiO_2 shell. At last, the large accumulations of e$^-$ and h$^+$ in the two interfaces of SiO_2 shell result in the formation of built-in electric field which will prevent their further accumulations.

In the third step of the photo-catalytic progress, the degradation rate of dyes is determined by the generation rate of effective radicals produced by the electron acceptors, and these radicals are directly responsible for the oxidative degradation [34]. So the role of electron acceptors is critical in enhancing the overall photo-degradation efficiency. Although dissolved oxygen molecules can serve as the electron acceptor in most photo-catalytic reaction [35], the presence of better electron acceptors is still desired for higher efficiency. The usage of H_2O_2 in photo-catalytic reaction can increase the formation rate of hydroxyl radicals [5,36,37] and then accelerate both the photo-degradation and mineralization of the organic compounds [38]. The $^\bullet$OH produced by H_2O_2 and the O_2^- generated from O_2 all participate in destroying the structure of the dyes in the catalytic reaction [12,39]. Since MO is an azo dye, the conjugative system and aryl rings are the main chromophores of MO, the degradation of MO is mainly caused by the damage of conjugative system and the –N=N– bond [12].
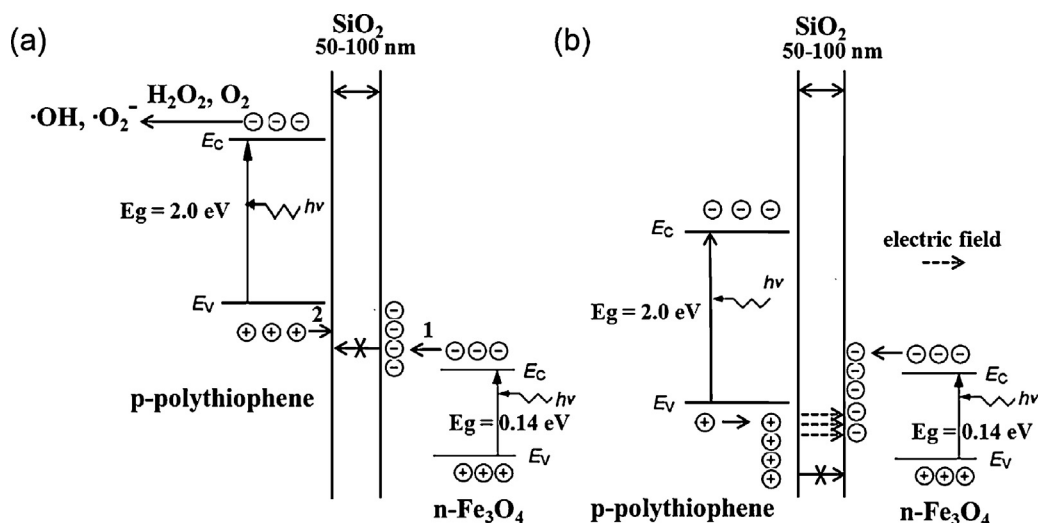
Fig. 8. The energy band diagram of the SIS structure and the transfer of light generated electrons and holes in the (a) initial and (b) later period of photo-catalytic reaction.
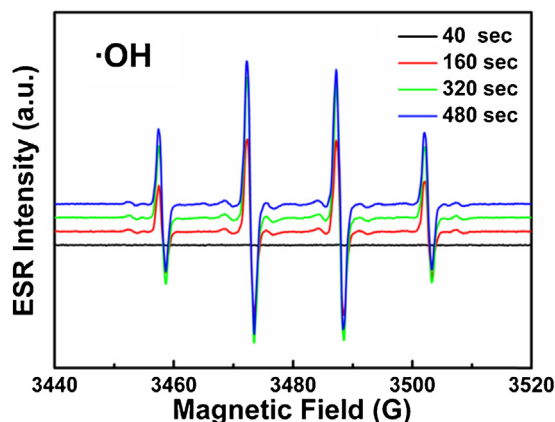

Fig. 9. The ESR spectra for the DMPO-containing suspensions of the FSP catalytic system with UV irradiation, $C_{(catalyst)} = 40$ mg/L, $C_{(MO)} = 50$ mg/L.

To further confirm the existence of active radicals in the process of photo-catalytic degradation, we investigated the ESR spectra in the same conditions of the photo-degradation reaction (Fig. 9). The characteristic 1:2:2:1 quartet signal was detected, indicating that the $^{\bullet}$OH radicals were generated during the photo-catalytic reaction. The signal intensity of the $^{\bullet}$OH radical showed an increase with the time lapsing in the first 480 s of the photo-catalytic reaction, revealing that more and more hydroxyl radicals were produced under the ultraviolet irradiation and hence MO could be degraded gradually by these radicals. Since the standard one electron reduction potential is -0.32 V for O_2 and 0.87 V for H_2O_2 (versus NHE), the H_2O_2 is thermodynamically a better electron acceptor than O_2. As expected, we detected more $^{\bullet}$OH radicals produced by H_2O_2 than O_2^- generated by O_2 (the signal of O_2^- is weak, and data not shown).

4. Conclusions

In this study, FSP SC with a SIS structure has been successfully prepared and characterized in detail. This multifunctional material presented a photo-catalytic rate constant of 0.02177 min^{-1} for MO which was 6.4, 1.6, and 2.5 times higher than that of FP, P, and TiO$_2$, respectively. The promoted photo-catalytic kinetics of FSP may be due to its SIS structure which was beneficial to the separation of photo-generated electrons and holes. The repetition experiments showed that the FSP had good stability and could be reused for ten cycles with only 14% decline of the photo-catalytic performance. In addition, the FSP SC could be easily reclaimed within 30 s using a common magnet, indicating potential application value. This work may lead to the development of new photo-catalysts by introduction of the SIS structure in the design of materials.

References

[1] H.J. Kim, A.R. Han, C.H. Cho, H. Kang, H.H. Cho, M.Y. Lee, J.M.J. Frechet, J.H. Oh, B.J. Kim, Chem. Mater. 24 (2012) 215–221.

[2] E.T. Niles, J.D. Roehling, H. Yamagata, A.J. Wise, F.C. Spano, A.J. Moule, J.K. Grey, J. Phys. Chem. Lett. 3 (2012) 259–263.

[3] N. Humphry-Baker, K. Driscoll, A. Rao, T. Torres, H.J. Snaith, R.H. Friend, Nano Lett. 12 (2012) 634–639.

[4] K. Yao, L. Chen, F. Li, P.S. Wang, Y.W. Chen, J. Phys. Chem. C 116 (2012) 714–721.

[5] S.T. Xing, Z.C. Zhou, Z.C. Ma, Y.S. Wu, Appl. Catal., B 107 (2011) 386–392.

[6] M. Bhaumik, T.Y. Leswifi, A. Maity, V.V. Srinivasu, M.S. Onyango, J. Hazard. Mater. 186 (2011) 150–159.

[7] L.G. Bach, M.R. Islam, J.T. Kim, S. Seo, K.T. Lim, Appl. Surf. Sci. 258 (2012) 2959–2966.

[8] S. Shin, H. Yoon, J. Jang, Catal. Commun. 10 (2008) 178–182.

[9] K. Takahashi, Y. Takano, T. Yamaguchi, J. Nakamura, C. Yokoe, K. Murata, Synth. Met. 155 (2005) 51–55.

[10] V.N. Antonov, B.N. Harmon, V.P. Antropov, A.Y. Perlov, A.N. Yaresko, Phys. Rev. B: Condens. Matter 64 (2001) 134410.

[11] S.K. Park, T. Ishikawa, Y. Tokura, Phys. Rev. B: Condens. Matter 58 (1998) 3717–3720.

[12] S.H. Xu, S.Y. Li, Y.X. Wei, L. Zhang, F. Xu, React Kinet., Mech. Catal. 101 (2010) 37–249.

[13] K. Ramamoorthy, M. Jayachandran, K. Sankaranarayanan, P. Misra, L.M. Kukreja, C. Sanjeeviraja, Sol. Energy 77 (2004) 193–201.

[14] A. Cheknane, J. Phys. D: Appl. Phys. 42 (2009) 115302.

[15] S.R. Vishwakarma, Rahmatullah, H.C. Prasad, J. Appl. Phys. 70 (1991) 7474–7477.

[16] F. Zhang, J. Lan, Z.S. Zhao, Y. Yang, R.Q. Tan, W.J. Song, J. Colloid Interface Sci. 387 (2012) 205–212.

[17] K.R. Reddy, K.P. Lee, J.Y. Kim, Y. Lee, J. Nanosci. Nanotechnol. 8 (2008) 5632–5639.

[18] L.A. Wang, K.G. Neoh, E.T. Kang, B. Shuter, Biomaterials 32 (2011) 2166–2173.

[19] A. Berlin, G. Zotti, S. Zecchin, G. Schiavon, M. Cocchi, D. Virgili, C. Sabatini, J. Mater. Chem. 13 (2003) 27–33.

[20] H. Zhang, X. Zhong, J.J. Xu, H.Y. Chen, Langmuir 24 (2008) 13748–13752.

[21] J.F. Guo, B.W. Ma, A.Y. Yin, K.N. Fan, W.L. Dai, Appl. Catal., B 101 (2011) 580–586.

[22] K. Takaoka, T. Otsuka, K. Naka, A. Niwa, T. Suzuki, C. Bureau, S. Maeda, K. Endo, D.P. Chong, J. Mol. Struct. 608 (2002) 175–182.

[23] F. Buckel, F. Effenberger, C. Yan, A. Golzhauser, M. Grunze, Adv. Mater. 12 (2000) 901–905.

[24] C. Jaegeun Noh, E. Ito, K. Nakajima, J. Kim, H. Lee, M. Hara, J. Phys. Chem. B 106 (2002) 7139–7141.

[25] D.L. Zhao, P. Teng, Y. Xu, Q.S. Xia, J.T. Tang, J. Alloys Compd. 502 (2010) 392–395.

[26] Y. Yang, H.W. Xiang, L. Tian, H. Wang, C.H. Zhang, Z.C. Tao, Y.Y. Xu, B. Zhong, Y.W. Li, Appl. Catal., A 284 (2005) 105–122.

[27] G. Liu, Q. Deng, H.Q. Wang, D.H.L. Ng, M.G. Kong, W.P. Cai, G.Z. Wang, J. Mater. Chem. 22 (2012) 9704–9713.

[28] B. Muktha, G. Madras, T.N. Guru Row, U. Scherf, S. Patil, J. Phys. Chem. B 111 (2007) 7994–7998.

[29] H. Tong, S.X. Ouyang, Y.P. Bi, N. Umezawa, M. Oshikiri, J.H. Ye, Adv. Mater. (2011) 1–23.

[30] S. Clement, F. Meyer, J. De Winter, O. Coulembier, C.M.L.V. Velde, M. Zeller, P. Gerbaux, J.Y. Balandier, S. Sergeyev, R. Lazzaroni, Y. Geerts, P. Dubois, J. Org. Chem. 75 (2010) 1561–1568.

[31] Y. Deng, D. Qi, C. Deng, X. Zhang, D. Zhao, J. Am. Chem. Soc. 130 (2008) 28–29.

[32] D.S. Sutar, S. Lenfant, D. Vuillaume, P. Yakhmi, Org. Electron. 9 (2008) 602–608.

[33] C.Y. Lin, Y.K. Fang, C.H. Kuo, S.F. Chen, C.S. Lin, T.H. Chou, Y.H. Lee, J.C. Lin, S.B. Hwang, Appl. Surf. Sci. 253 (2006) 898–903.

[34] H.C. Liang, X.Z. Li, Appl. Catal., B 86 (2009) 8–17.

[35] Y.G. Xu, H. Xu, H.M. Li, J.X. Xia, C.T. Liu, L. Liu, J. Alloys Compd. 509 (2011) 3286–3292.

[36] N.M. Mahmoodi, M. Aramia, J.S. Zhang, J. Alloys Compd. 509 (2011) 4754–4764.

[37] X.B. Hu, B.Z. Liu, Y.H. Deng, H.Z. Chen, S. Luo, C. Sun, P. Yang, S.G. Yang, Appl. Catal., B 107 (2011) 274–283.

[38] N. Wang, L.H. Zhu, Y.P. Huang, Y.B. She, Y.M. Yu, H.Q. Tang, J. Catal. 266 (2009) 199–206.

[39] C.C. Chen, X.Z. Li, W.H. Ma, J.C. Zhao, H. Hidaka, N. Serpone, J. Phys. Chem. B 106 (2002) 318–324.